SURFACE SCIENCE 36 (1973) 317-352 © North-Holland Publishing Co.

THE PHYSICAL INTERACTION OF GASES WITH CRYSTALLINE SOLIDS

I. GAS–SOLID ENERGIES AND PROPERTIES OF ISOLATED ADSORBED ATOMS*

WILLIAM A. STEELE

Department of Chemistry, The Pennsylvania State University, University Park, Pennsylvania, 16802, U.S.A.

Received 21 April 1972; revised manuscript received 11 September 1972

It is shown that the potential energy of a gas atom interacting with a solid having a surface made up of single type of exposed lattice plane can be expressed as a Fourier series in the position variables in the plane parallel to the surface. Assuming that the total interaction is a pair-wise sum of gas atom–solid atom terms, an analytic expression for the Fourier coefficients is obtained for inverse power law interactions that is a generalization of an earlier result of Hove and Krumhansl. Gas–solid potentials calculated for several surface lattices by direct summation are compared with those given by the truncated Fourier series, and it is concluded that a satisfactory representation of the energy is obtained even when the number of terms included is small. The truncated series is then utilized to calculate Henry's Law adsorption constants and average energies for an isolated adsorbed atom. These results are compared with calculations based on completely localized and perfectly mobile adsorption models.

1. Introduction

The energy of a single gas atom interacting with a solid adsorbent is a quantity of fundamental interest in the statistical mechanical theory of adsorption. It determines the characteristics of atomic or molecular elastic scattering from solid surfaces, and is of major importance in calculations of inelastic scattering; in addition, statistical computations[1,2]) of the thermodynamic properties of adsorbed atoms are based on various well-known integrals of functions of the gas–solid potential for isolated atoms, and the gas–solid plus the gas–gas energy for clusters of interacting atoms on the surface. For many years, the dependence of this gas–solid potential has been idealized either by assuming that it depended only upon the perpendicular gas–solid distance and not at all upon τ, the two-dimensional vector parallel to the surface (perfectly mobile adsorbed layer), or by assuming that the adsorbed atoms were localized in the vicinity of one of the minima in the

* This work supported by a grant from the Army Research Office – Durham.

potential surface so that the energy could be represented by the expression for a three-dimensional harmonic oscillator for all physically interesting values of the position vector $\boldsymbol{r}_i$ of the ith molecule. In this paper, it will be assumed that the physical interaction energy $u_s(\boldsymbol{r}_i)$ for the ith gas atom at a position $\boldsymbol{r}_i$ relative to some origin located at an arbitrary point in the solid can be represented as a sum of pair-wise energies. Thus, if $e_{gs}(\rho_{ij})$ is the interaction of the ith gas atom with jth atom (or molecule) located in the solid at a distance of ρ_{ij} from the gas atom, one has

$$u_s(\boldsymbol{r}_i) = \sum_j e_{gs}(\rho_{ij}). \tag{1.1}$$

This sum depends not only upon the parameters and functional dependence of $e_{gs}(\rho_{ij})$, but also upon the arrangement of the molecules in the solid; that is, it is a function of the solid lattice symmetry and spacing. Indeed, $u_s(\boldsymbol{r}_i)$ is sensitive primarily to the symmetry and spacing in the exposed plane of atoms, since it is this surface plane which is closest to the gas atom and which consequently interacts most strongly with it. With the advent of electronic computers, the sum in eq. (1.1) has been performed as a function of perpendicular distance z for a number of lattices and for a number of gas–solid positions relative to the lattice[3]). In these calculations, it has generally been assumed that the gas is made up of spherically symmetric entities. In this case, only dispersion and electronic overlap forces are important, and one can represent $e_{gs}(\rho_{ij})$ by a function such as the Lennard-Jones 12–6 expression:

$$e_{gs}(\rho_{ij}) = 4\varepsilon_{gs}\left\{\left(\frac{\sigma_{gs}}{\rho_{ij}}\right)^{12} - \left(\frac{\sigma_{gs}}{\rho_{ij}}\right)^{6}\right\}. \tag{1.2}$$

When these sums are performed for reasonable values of the parameters, it is found that potentials that give rise to the completely localized or the perfectly mobile models are not particularly good representations of the actual situation; consequently, the applicability of calculations of thermodynamic quantities based on these models comes into question. These quantities include observables such as the Henry's Law constant K_H. Experimentally, this constant is obtained from an adsorption isotherm by evaluating

$$K_H = \lim_{p\to 0}\left(\frac{n_a}{p}\right), \tag{1.3}$$

where n_a is the moles adsorbed at pressure p. Theoretically, K_H can be calculated from[2,4])

$$K_H = \frac{1}{kT}\int_V \left[\exp\left(\frac{-u_s(\boldsymbol{r})}{kT}\right) - 1\right] d\boldsymbol{r}, \tag{1.4}$$

where V is the gas space volume in the adsorption container. Thus, the Henry's Law constant is dependent upon the interaction of an isolated atom with the surface. One other such observable is the isosteric heat q_{st} in the limit of zero coverage. Although this heat is defined as the difference between the molar enthalpy of the gas and the partial molar enthalpy of the adsorbed material, a derivation similar to that leading to the Clausius–Clapeyron equation gives[2,4])

$$\lim_{n_a \to 0} \left(\frac{q_{st}}{R}\right) = \left(\frac{\partial \ln K_H}{\partial (1/T)}\right) - T . \tag{1.5a}$$

From eq. (1.4), one has

$$-k\left[\left(\frac{\partial \ln K_H}{\partial (1/T)}\right) - T\right] = \frac{\int_V u_s(\boldsymbol{r}) \exp[-u_s(\boldsymbol{r})/kT]\, d\boldsymbol{r}}{\int_V \{\exp[-u_s(\boldsymbol{r})/kT] - 1\}\, d\boldsymbol{r}} . \tag{1.5b}$$

The expression on the right hand side of eq. (1.5b) is just equal to the average potential energy $\langle u_s \rangle$ of an isolated atom on the surface.

Of course, the computer results for $u_s(\boldsymbol{r})$ that are given in the form of tables of numbers for various discrete values of $\boldsymbol{r}$ are not particularly convenient for use in integrations such as those of eqs. (1.4) or (1.5b). It is particularly difficult to use these results in a systematic study of the effects of surface lattice symmetry and size upon thermodynamic properties such as the Henry's Law constant and the limiting isosteric heat. Although a few calculations of this type have been reported[5]), they are too limited in scope and involve too many approximations to lead to any useful conclusions, except possibly that an analytic representation of $u_s(\boldsymbol{r})$ is a prequisite for further progress in this work.

There are a variety of related problems whose solutions would be greatly facilitated if an analytic representation of $u_s(\boldsymbol{r})$ were available. For example, a number of papers have appeared in which the bound state energies of an isolated helium atom adsorbed on either a rare gas crystal surface or an exposed graphite basal plane were computed[6,7]); these calculations have recently been extended to deal with neon and argon atoms adsorbed on xenon surfaces[6]). In all these studies, the wave functions and energy levels of the isolated adsorbed atoms were evaluated by the variational method; that is, the ground state wave function was expressed as a linear combination of some suitable set of basis functions $\phi_l(\boldsymbol{r})$. The expectation value of the energy was calculated by evaluating matrix elements such as $\langle \phi_l(\boldsymbol{r})\, u_s(\boldsymbol{r})\, \phi_l(\boldsymbol{r}) \rangle$ and then choosing a set of coefficients that minimizes the sum of the matrix elements. Of course, the fact that $u_s(\boldsymbol{r})$ is available only in the tabular form

greatly increases the cost of calculating a matrix element as well as introducing an element of uncertainty in the result.

Another well-known problem that requires a knowledge of the gas–surface potential for its successful solution is that of the angular distribution of atoms when a molecular beam is scattered from a solid surface. Indeed, the calculation of even a single trajectory for a molecule with given incident velocity and position relative to the surface lattice is a lengthy process, especially if inelastic effects are important. Since the observed scattering is an average over all positions and a distribution of velocities, many such trajectories are required. Consequently, these calculations have been successful to date only by introducing such an extremely simple form for $u_s(\boldsymbol{r})$[8]) that quantitative comparisons between experiment and theory are effectively precluded. As a particular example, consider the scattering of helium from single crystal surfaces. One can begin by calculating the scattering in terms of the quantum mechanical phase shifts associated with the unbound states of a helium atom interacting with the solid. Indeed, a detailed formal theory of the elastic scattering (diffraction) of light atoms has been presented by Cabrera, Celli, Goodman and Manson[8]), together with some analysis of inelastic scattering processes. Once again, the application of this theory to real systems would be greatly facilitated if an analytic form of $u_s(\boldsymbol{r})$ were available, particularly if $u_s(\boldsymbol{r})$ was expressed as a Fourier series in τ.

Oddly enough, this problem was treated and solved for surface lattices of square symmetry in 1953 by Hove and Krumhansl[9]). Conceivably, the reason that subsequent workers have ignored this approach to the problem[10]) is a lack of knowledge concerning the accuracy of the analytic results. Although Hove and Krumhansl succeeded in giving explicit expressions for the z-dependent coefficients in a Fourier expansion for $u_s(z, \tau)$, this calculation is not particularly useful unless the infinite Fourier series can be truncated after a moderate number of terms without appreciable loss of accuracy. In 1953, computer results that would allow one to compare the exact $u_s(\boldsymbol{r})$ with curves calculated from the truncated series were almost non-existent. In the present paper, we present a number of such comparisons which indicate that one can indeed represent $u_s(\boldsymbol{r})$ by Fourier series that has been truncated after a few terms. In addition, Hove and Krumhansl's theory is extended to surface lattices of arbitrary symmetry. Finally, the Fourier expansions for $u_s(\boldsymbol{r})$ are utilized to compute K_H and $\langle u_s \rangle$ for gases interacting with lattices of varying symmetry and relative size. In this way, the accuracy of the localized and mobile models as descriptions of adsorption on real crystal lattices can be tested. Evidently, these results will also be helpful in developing theories of physical adsorption which need not invoke either of these simplifications. In future papers, the analytic gas–solid potential will be

utilized in calculations of other properties such as the interactions of pairs and triplets of adsorbed molecules, and molecular beam elastic scattering.

2. Theory

We consider first the surface layer of atoms in a perfectly crystalline solid, and define a two-dimensional lattice vector parallel to this layer by:

$$\boldsymbol{l} = l_1\boldsymbol{a}_1 + l_2\boldsymbol{a}_2\,, \tag{2.1}$$

where l_1 and l_2 are integers and $\boldsymbol{a}_1$ and $\boldsymbol{a}_2$ are the unit lattice vectors in two dimensions. Thus, one has the usual property that the translation of a gas atom by $\boldsymbol{l}$ will carry it from one position above a surface lattice cell into an equivalent position above a different lattice cell. Consequently,

$$u_s(\boldsymbol{r} + \boldsymbol{l}) = u_s(\boldsymbol{r})\,. \tag{2.2}$$

Addition of $\boldsymbol{l}$ to $\boldsymbol{r}$ evidently leaves the perpendicular gas–solid distance z unchanged. Just as in the theory of three-dimensional crystals, the length and orientation of $\boldsymbol{a}_1$ and $\boldsymbol{a}_2$ are arbitrary to some extent. These vectors define a rhombus (of area $|\,\boldsymbol{a}_1 \times \boldsymbol{a}_2\,|$ in the general case) which is at least large enough to cover an array of atoms that allows one to generate the entire surface by replicating those in the unit cell. The natural way of representing a periodic function such as $u_s(\boldsymbol{r})$ is a Fourier series:

$$u_s(\boldsymbol{r}) = \sum_{\boldsymbol{g}} w_{\boldsymbol{g}}(z) \exp(i\boldsymbol{g}\cdot\boldsymbol{\tau})\,, \tag{2.3}$$

where $\boldsymbol{\tau}$ is the two-dimensional translation vector and $\boldsymbol{g}$ is a multiple of the reciprocal lattice vectors $\boldsymbol{b}_1$ and $\boldsymbol{b}_2$:

$$\boldsymbol{g} = 2\pi[g_1\boldsymbol{b}_1 + g_2\boldsymbol{b}_2]\,. \tag{2.4}$$

In this expression, g_1 and g_2 are integers and $\boldsymbol{b}_1$ and $\boldsymbol{b}_2$ are defined in the usual way:

$$\boldsymbol{a}_1\cdot\boldsymbol{b}_1 = 1 = \boldsymbol{a}_2\cdot\boldsymbol{b}_2\,, \quad \boldsymbol{a}_1\cdot\boldsymbol{b}_2 = 0 = \boldsymbol{a}_2\cdot\boldsymbol{b}_1\,. \tag{2.5}$$

Eq. (2.5) means that $\boldsymbol{b}_1$, $\boldsymbol{b}_2$ define a rhombus with sides perpendicular to $\boldsymbol{a}_2$, $\boldsymbol{a}_1$ and of length $\csc\phi/a_1$, $\csc\phi/a_2$, where ϕ is the angle between $\boldsymbol{a}_1$ and $\boldsymbol{a}_2$. Eq. (2.3) conforms to the periodicity property of $u_s(\boldsymbol{r})$ given in eq. (2.2); in addition, we can choose the origin of the lattice vector so that $w_{\boldsymbol{g}}(z) = w_{-\boldsymbol{g}}(z)$ and $u_s(\boldsymbol{r})$ is real. Eq. (2.3) can also be written as

$$u_s(\boldsymbol{r}) = \sum_{\boldsymbol{g}}\sum_{\alpha} w_{\boldsymbol{g}}(z_\alpha) \exp(i\boldsymbol{g}\cdot\boldsymbol{\tau})\,, \tag{2.6}$$

where

$$w_{\boldsymbol{g}}(z_\alpha) = \frac{1}{a_s}\int_{\boldsymbol{a}} \exp(-i\boldsymbol{g}\cdot\boldsymbol{\tau})\, u_s(z_\alpha, \tau)\, d\tau. \tag{2.7}$$

Here, $w_{\boldsymbol{g}}(z_\alpha)$ is the Fourier coefficient for the αth plane of atoms located at a distance z_α from the gas atom, a_s is the area of the unit lattice cell, and $\boldsymbol{a}$ denotes the limits of the integration variable τ.

We now introduce the pair-wise additivity approximation of eq. (1.1) for $u_s(z_\alpha, \tau)$:

$$u_s(z_\alpha, \tau) = \sum_{l_1, l_2}\sum_k e_{gs}(z_\alpha, \tau + \boldsymbol{l} + \boldsymbol{m}_k), \tag{2.8}$$

where $\boldsymbol{l}+\boldsymbol{m}_k$ is a vector that gives the location of the kth atom in the unit cell whose location is given by $\boldsymbol{l}$. We define a vector $\boldsymbol{t}=\boldsymbol{\tau}+\boldsymbol{l}+\boldsymbol{m}_k$ and write eq. (2.7) as

$$w_{\boldsymbol{g}}(z_\alpha) = \frac{1}{a_s}\sum_k \exp(i\boldsymbol{g}\cdot\boldsymbol{m}_k)\int_{\mathscr{A}} \exp(-i\boldsymbol{g}\cdot\boldsymbol{t})\, e_{gs}(z_\alpha, \boldsymbol{t})\, d\boldsymbol{t}, \tag{2.9}$$

where $\mathscr{A}$ is now the entire area of the αth plane.

Further progress requires that we specify e_{gs} to some extent and we thus assume that it is a function only of the separation distance $\rho=(z_\alpha^2+t^2)^{\frac{1}{2}}$. In this case, we can integrate over the orientation of τ to obtain

$$w_{\boldsymbol{g}}(z_\alpha) = \frac{2\pi}{a_s}\sum_k \exp(i\boldsymbol{g}\cdot\boldsymbol{m}_k)\int_0^\infty J_0(gt)\, e_{gs}(\rho)\, t\, dt. \tag{2.10}$$

If $e_{gs}(\rho)$ has an inverse power dependence on ρ such as in the Lennard-Jones potential of eq. (1.2), the remaining integration of eq. (2.10) is readily performed since

$$\int_0^\infty J_0(gt)\left(\frac{1}{z^2+t^2}\right)^{n+1} t\, dt = \frac{1}{n!}\left(\frac{g}{2z}\right)^n K_n(gz), \tag{2.11}$$

where K_n is the modified Bessel function of the second kind. One can evaluate the term with $\boldsymbol{g}=\boldsymbol{0}$ by means of the relation

$$\lim_{g\to 0}\frac{1}{n!}\left(\frac{g}{2z}\right)^n K_n(gz) = \frac{1}{2nz^{2n}}, \quad n>0. \tag{2.12}$$

Thus, for the 12–6 potential, we can combine eqs. (1.2), (2.6), (2.10) and

2.11) to obtain

$$\frac{u_s(r)}{\varepsilon_{gs}} = \frac{2\pi}{a_s}\sum_{\alpha}\left\{q\left(\frac{2}{5}\frac{\sigma_{gs}^{12}}{z_\alpha^{10}} - \frac{\sigma_{gs}^{6}}{z_\alpha^{4}}\right) + \sum_{g\neq 0}\sum_{k=1}^{q}\exp(i\boldsymbol{g}\cdot[\boldsymbol{m}_k + \boldsymbol{\tau}]) \times\left(\frac{\sigma_{gs}^{12}}{30}\left(\frac{g}{2z_\alpha}\right)^5 K_5(gz_\alpha) - 2\sigma_{gs}^{6}\left(\frac{g}{2z_\alpha}\right)^2 K_2(gz_\alpha)\right)\right\}, \tag{2.13}$$

where q is the total number of atoms per unit surface cell. This is the result that we wish to exploit in this and subsequent papers; it represents an extension of Hove and Krumhansl's theory for a square surface lattice; it is easily generalized to solids containing several types of interacting group, since the only change required is the insertion of differing values of $\varepsilon_{gs}(k)$ and $\sigma_{gs}(k)$ for the kth atom in the unit surface cell. Another generalization of eq. (2.13) can be made when the atoms in an underlying layer are at different positions than those in the first layer; if this is the case, one defines q_α to be the total number of atoms in the projection of the unit cell in the αth layer, and $\boldsymbol{m}_k(\alpha)$ to be the position vectors of these atoms.

As an example of the utility of the general approach, it is interesting to see how the calculation of the electrostatic potential near the surface of the (100) face of the NaCl-type crystal that was first given by Lennard-Jones and Dent[11]) can be rederived. Inasmuch as the electrostatic potential $\Phi(\boldsymbol{r})$ is the coulomb energy of a test charge, one has

$$\Phi(\boldsymbol{r}) = \sum_n\sum_i \frac{e_n}{\rho_{ni}}, \tag{2.14}$$

where e_n is the charge of the nth kind of ion in the solid, and ρ_{ni} is the distance between the test charge and the ith ion of type n. The potential is written as

$$\Phi(\boldsymbol{r}) = \sum_{\boldsymbol{g}}\sum_n\sum_\alpha w_{\boldsymbol{g}}^{(n)}(z_\alpha)\exp[i\boldsymbol{g}\cdot(\boldsymbol{\tau} - \boldsymbol{\tau}_n(\alpha))]. \tag{2.15}$$

Thus

$$w_{\boldsymbol{g}}(z_\alpha) = \sum_n w_{\boldsymbol{g}}^{(n)}(z_\alpha)\exp[-i\boldsymbol{g}\cdot\boldsymbol{\tau}_n(\alpha)],$$

where $\boldsymbol{\tau}_n(\alpha)$ denotes the position of the nth ion in the lattice cell which is in a plane at a distance z_α from the test charge. If one follows the argument leading to eq. (2.10), it can be shown that the coefficient $w_{\boldsymbol{g}}^{(n)}(z_\alpha)$ is given by:

$$w_{\boldsymbol{g}}^{(n)}(z_\alpha) = \frac{2\pi e_n}{a_s}\int_0^\infty J_0(gt)\left(\frac{1}{z_\alpha^2 + t^2}\right)^{\frac{1}{2}} t\,dt. \tag{2.16}$$

In other words, the Coulomb interaction is an inverse power law energy such that $e_{gs}=e_n/(z_\alpha^2+t^2)^{\frac{1}{2}}$ for the nth type of atom in the αth plane. When the integration in eq. (2.16) is performed, one can use the fact that $K_{-\frac{1}{2}}(x)=$ $=(\pi/2x)^{\frac{1}{2}}e^{-x}$ to write:

$$w_g^{(n)}(z_\alpha)=\left(\frac{2\pi e_n}{a_s}\right)\left(\frac{1}{g}\right)\exp(-gz_\alpha). \tag{2.17}$$

Although eq. (2.17 makes it appear that an infinite contribution is obtained when $g=0$, it should be noted that such a term in the expression for the potential is independent of both structure and distance (τ and z); the requirement of charge neutrality in the solid causes these terms to give a zero contribution to the potential when summed over all e_n. [This result is confirmed by the alternative calculation based on a solution of the Poisson equation[11]).]

When eq. (2.17) is substituted into eq. (2.15), one finds

$$\Phi(\boldsymbol{r})=\frac{2\pi}{a_s}\sum_\alpha\sum_n\sum_{g\neq 0}\left(\frac{e_n}{g}\right)\exp[i\boldsymbol{g}\cdot(\boldsymbol{\tau}-\boldsymbol{\tau}_n(\alpha))-gz_\alpha]. \tag{2.18}$$

In the case of the exposed (100) face of NaCl lattice, there are two different types of plane parallel to the surface. If a negative ion is placed at the origin of τ in the outermost plane (denoted by $\alpha=1$), one has

$$\left.\begin{aligned} &=-e,\ \alpha\text{ odd}\\ e_n&=+e,\ \alpha\text{ even}\end{aligned}\right\}\ \text{at } \tau_n=0,\ 0 \text{ and } \tfrac{1}{2}a,\ \tfrac{1}{2}a; \tag{2.19a}$$

$$\left.\begin{aligned} &=+e,\ \alpha\text{ odd}\\ e_n&=-e,\ \alpha\text{ even}\end{aligned}\right\}\ \text{at } \tau_n=0,\ \tfrac{1}{2}a \text{ and } \tfrac{1}{2}a,\ 0. \tag{2.19b}$$

The sums over α and n in eq. (2.18) can be performed for the ion positions given by eq. (2.19); one finds

$$\begin{aligned}\Phi(\boldsymbol{r})=-\frac{2\pi e}{a^2}\sum_{g_1,g_2\neq 0}\frac{e^{-gz}}{g(1+e^{-\frac{1}{2}g})}\{&\cos[2\pi(g_1s_1-g_2s_2)]\\ &+\cos[2\pi(g_1(s_1-\tfrac{1}{2})+g_2(s_2-\tfrac{1}{2}))]-\cos[2\pi(g_1(s_1-\tfrac{1}{2})+g_2)]\\ &-\cos[2\pi(g_1s_1+g_2(s_2-\tfrac{1}{2}))]\},\end{aligned} \tag{2.20}$$

where $s_1=x/a$, $s_2=y/a$, $a_s=a^2$, and $g=(2\pi/a)\,(g_1^2+g_2^2)^{\frac{1}{2}}$.

Since g_1 and g_2 are integers, one can simplify the expression in the curly brackets to give

$$\Phi(\boldsymbol{r})=\frac{8\pi e}{a^2}\sum_{g_1,g_2}{}'\frac{(-1)^{\frac{1}{2}(g_1+g_2)}e^{-gz}}{g(1+e^{-\frac{1}{2}g})}\cos[2\pi(g_1(s_1-\tfrac{1}{4})+g_2(s_2-\tfrac{1}{4}))], \tag{2.21}$$

with the prime on the sum used to indicate that only odd values of g_1 and g_2 are to be included.

Eq. (2.21) is equivalent to the previous result for the Coulomb potential near the surface of a NaCl crystal with an exposed (100) face; furthermore, it is evident that this technique can readily be applied to other crystals and other exposed lattice planes by making the appropriate modifications in the ionic positions and charges given in eq. (2.19).

Returning now to the case where the interactions are Lennard-Jones 12–6 functions, we note that the Bessel functions $K_n(x)$ decay quite rapidly with x, and have the asymptotic form:

$$\lim_{x\to\infty} K_n(x) = \left(\frac{\pi}{2x}\right)^{\frac{1}{2}} e^{-x}. \tag{2.22}$$

Explicit calculations show that the τ-dependent terms that make an appreciable contribution to the gas–solid energy over the physically relevant range of z are often limited to those that arise from the surface plane only (i.e., when $z_\alpha = z$, the perpendicular gas–surface distance). In this case, eq. (2.13) can be simplified to:

$$\frac{u_s(\boldsymbol{r})}{\varepsilon_{gs}} = \frac{2\pi A^6}{a_s^*}\left\{q\sum_\alpha\left(\frac{2A^6}{5z_\alpha^{*10}} - \frac{1}{z_\alpha^{*4}}\right) + \sum_{g=0}\sum_{k=1}^{q}\exp\left(i\boldsymbol{g}^*\cdot[\boldsymbol{m}_k^* + \boldsymbol{\tau}^*]\right)\right.$$
$$\left.\times\left[\frac{A^6}{30}\left(\frac{g^*}{2z^*}\right)^5 K_5(g^*z^*) - 2\left(\frac{g^*}{2z^*}\right)^2 K_2(g^*z^*)\right]\right\}, \tag{2.23}$$

where we have shifted to a set of reduced variables by defining:

$$\begin{aligned} a_s^* &= a_s/a_1^2, \\ z^* &= z/a_1, \\ g^* &= g a_1, \\ A &= \sigma_{gs}/a_1. \end{aligned} \tag{2.24}$$

The reduced vector parallel to the surface $\boldsymbol{\tau}^*$ can of course be expressed as a function of the cartesian coordinates x, y; however, we will see later that it is often most convenient to write it in terms of the lattice vectors $\boldsymbol{a}_1$, $\boldsymbol{a}_2$. That is, one can write

$$\boldsymbol{\tau} = s_1\boldsymbol{a}_1 + s_2\boldsymbol{a}_2, \tag{2.25}$$

where s_1 and s_2 range from 0 to 1 as the position of a gas atom moves over a unit surface lattice cell. This choice of coordinate system has the advantage that

$$\boldsymbol{g}^*\cdot\boldsymbol{\tau}^* = 2\pi(g_1s_1 + g_2s_2). \tag{2.26}$$

The analytic expression for $u_s(r)$ that is given in eq. (2.23) can be compared to a well-known and widely used approximation obtained when one replaced the sum of pair-wise interactions by an integration over the solid phase:

$$\frac{u_s(r)}{\varepsilon_{gs}} = 8\pi\rho_s \int_z^\infty dz' \int_0^\infty t\, dt \left(\frac{\sigma_{gs}^{12}}{(z'^2+t^2)^6} - \frac{\sigma_{gs}^6}{(z'^2+t^2)^3} \right), \tag{2.27}$$

where ρ_s is the number density of atoms in the solid. If one integrates over t, the distance variable in the surface plane, eq. (2.27) becomes

$$\frac{u_s(r)}{\varepsilon_{gs}} = 2\pi\rho_s \int_z^\infty dz' \left(\frac{2}{5} \frac{\sigma_{gs}^{12}}{z'^{10}} - \frac{\sigma_{gs}^6}{z'^4} \right). \tag{2.28}$$

If we write $\rho_s = (q/a_s\,\Delta z)$, where Δz is the distance between the discrete planes in a real solid, the integral over z' in eq. (2.28) can be converted into a sum over planes which is identical to the leading term on the right-hand side of eq. (2.13). On the other hand, one can proceed with the integration in eq. (2.28) to find

$$\begin{aligned} \frac{u_s(r)}{\varepsilon_{gs}} &= \frac{2\pi\rho_s}{3} \left[\frac{2}{15} \frac{\sigma_{gs}^{12}}{z^9} - \frac{\sigma_{gs}^6}{z^3} \right] \\ &= \frac{2\pi\rho_s^* A^6}{3} \left[\frac{2}{15} \frac{A^6}{z^{*9}} - \frac{1}{z^{*3}} \right], \end{aligned} \tag{2.29}$$

where $\rho_s^* = \rho_s a_1^3$. Actual calculations show that the integrated energy given by eq. (2.29) is very poor representation of $u_s(r)$ for energies near the minimum.

Energies have been computed for atoms over surfaces made up of the (100) and (111) planes for fcc crystal, and of the graphite basal plane by direct summation of pair-wise energies for three positions of the adsorbed atom. These positions are denoted by S, SP and A, and are shown in fig. 1, together with the unit lattice cells for the three surfaces treated. The points denoted by A correspond to the positions of the atoms in the surface lattice; those denoted by SP are saddle points in the potential energy surface and represent the low points in the energy barriers that separate adsorption sites S where the gas–solid energy is a minimum. The unit cells for the (111) face fcc lattice and the graphite basal plane have identical symmetries, but differ in the number of surface atoms per unit cell, the location of the atoms and sites, and the lengths of the reduced vectors a_1^* and a_2^*. In fact, for both fcc lattices,

$$a_1 = a_2 = \sigma_{ss}, \tag{2.30a}$$

where σ_{ss} is the nearest neighbor distance in the solid. For the graphite basal plane, one has

$$a_1 = a_2 = \sqrt{3}\,\sigma_{ss}. \tag{2.30b}$$

If we write the atomic positions in terms of $\tau = s_1 a_1 + s_2 a_2$, one finds atoms at $s_1, s_2 = 0,0;\ 1,0;\ 0,1;\ 1,1$ for the fcc lattices (but only one atom per unit cell), and at $s_1, s_2 = \frac{1}{3}, \frac{1}{3};\ \frac{2}{3}, \frac{2}{3}$ for the graphite basal plane (two atoms per unit cell).

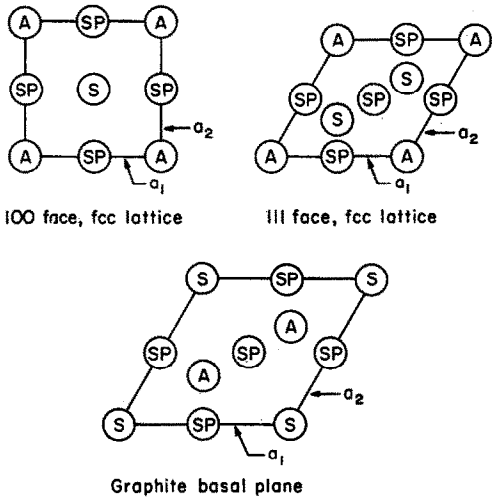

Fig. 1. Surface unit lattice cells for the crystals considered in this paper. The points denoted by A indicate the positions of the atoms in the surface planes of the solids; adsorption sites are denoted by S, and the saddle-points in the potential functions by SP. The lattice vectors a_1 and a_2 are also shown.

Thus

$$\sum_{k=1}^{q} \exp(i\boldsymbol{g}\cdot[\boldsymbol{m}_k + \boldsymbol{\tau}] = \begin{cases} \exp(i\boldsymbol{g}\cdot\boldsymbol{\tau}) & \text{(fcc lattices)} \\ 2\cos[\tfrac{2}{3}\pi(g_1 + g_2)]\exp(i\boldsymbol{g}\cdot\boldsymbol{\tau}) & \text{(graphite basal plane)} \end{cases} \tag{2.31}$$

Finally, the lengths of the reduced $\boldsymbol{g}$ vectors are given by

$$g^* = \begin{cases} \dfrac{4\pi}{\sqrt{3}}[g_1^2 + g_2^2 - g_1 g_2]^{\frac{1}{2}} & \text{((111) face, fcc and graphite basal plane)} \\ 2\pi(g_1^2 + g_2^2)^{\frac{1}{2}} & \text{((100) face, fcc)} \end{cases} \tag{2.32}$$

We are now in a position to write explicit expressions for the gas–solid energy of an atom over the three lattices considered here. In particular, if

we define $u_s^* = u_s(\boldsymbol{r})/\varepsilon_{gs}$, we have

$$u_s^* = E_0(z^*) + \sum_{n>0} E_n(z^*) f_n(s_1, s_2), \tag{2.33}$$

with

$$E_0(z^*) = \frac{2\pi q A^6}{a_s^*} \sum_{p=0}^{\infty} \left(\frac{2A^6}{5(z^* + p\Delta z^*)^{10}} - \frac{1}{(z^* + p\Delta z^*)^4} \right), \tag{2.34}$$

where p is an integer and Δz^* is the reduced distance between planes. Also,

$$E_n(z^*) = \frac{2\pi A^6}{a_s^*} \left[\frac{A^6}{30} \left(\frac{g_n^*}{2z^*} \right)^5 K_5(g_n^* z^*) - 2 \left(\frac{g_n^*}{2z^*} \right)^2 K_2(g_n^* z^*) \right]. \tag{2.35}$$

Values of q, a_s^*, g_n^* and f_n are listed in table 1 for n up to five for the three lattices treated in this paper. Finally, we note that one can use cartesian coordinates x, y rather than the lattice symmetry coordinates $s_1 \boldsymbol{a}_1$, $s_2 \boldsymbol{a}_2$ if one writes

$$\left.\begin{aligned} \boldsymbol{g}^* \cdot \boldsymbol{\tau}^* &= 2\pi(g_1 x_1^* + g_2 y_2^*) && ((100)\text{ face, fcc}) \\ &= 2\pi \left[\frac{x^*}{\sqrt{3}} (2g_2 - g_1) + g_2 y^* \right] && ((111)\text{ face, fcc and graphite basal plane}) \end{aligned}\right\} \tag{2.36}$$

in place of eq. (2.26). [In eq. (2.36), we have taken the y-coordinate to be parallel to the $\boldsymbol{a}_2$ vector.]

Having obtained an explicit analytic expression for the energy, we can now utilize it to calculate quantities of interest such as K_H and $\langle u_s \rangle$. When eq. (2.33) is substituted into eqs. (1.4) and (1.5), further progress is facilitated if one realizes that the τ-dependent terms are important only over a short range of distance z^* (as is illustrated in fig. 10.) Even though these terms in the energy become quite large as the gas–solid distance becomes smaller than that for the minimum energy, the total interaction energy becomes large and positive for all τ due to the rapid rise of $E_0(z^*)$. Since the integrands in eqs. (1.4) and (1.5) involve $\exp[-u_s(\boldsymbol{r})/kT]$, they are of negligible importance when the energy is large and positive. If we now consider the calculation of K_H, we can express the element of integration in terms of the lattice symmetry coordinates by writing:

$$K_H = \frac{n_s a_s^* a_1^3}{kT} \int_0^1 \int_0^1 \int_0^{\infty} \left[\exp\left(\frac{-u_s^*}{T^*} \right) - 1 \right] ds_1 \, ds_2 \, dz^*. \tag{2.37}$$

where $T^* = kT/\varepsilon_{gs}$ and n_s is the total number of lattice sites in the surface.

TABLE 1

Terms in the Fourier series expression for the gas–solid energies for specific lattices

n	$g_n^*/2\pi$	$f_n(s_1, s_2)/2$
	(a) 100 face, fcc lattice: $q=1$, $a_s^*=1$, $\Delta z^*=1/\sqrt{2}$	
1	1	$\cos 2\pi s_1+\cos 2\pi s_2$
2	$\sqrt{2}$	$\cos 2\pi(s_1+s_2)+\cos 2\pi(s_1-s_2)$
3	2	$\cos 4\pi s_1+\cos 4\pi s_2$
4	$\sqrt{5}$	$\cos 2\pi(2s_1+s_2)+\cos 2\pi(s_1+2s_2)$ $+\cos 2\pi(2s_1-s_2)+\cos 2\pi(s_1-2s_2)$
5	$2\sqrt{2}$	$\cos 4\pi(s_1+s_2)+\cos 4\pi(s_1-s_2)$
	(b) 111 face, fcc lattice: $q=1$, $a_s^*=\sqrt{3}/2$, $\Delta z^*=\sqrt{2/3}$	
1	$2/\sqrt{3}$	$\cos 2\pi s_1+\cos 2\pi s_2+\cos 2\pi(s_1+s_2)$
2	2	$\cos 2\pi(s_1+2s_2)+\cos 2\pi(2s_1+s_2)+\cos 2\pi(s_1-s_2)$
3	$4/\sqrt{3}$	$\cos 4\pi s_1+\cos 4\pi s_2+\cos 4\pi(s_1+s_2)$
4	$2\sqrt{7/3}$	$\cos 2\pi(3s_1+s_2)+\cos 2\pi(s_1+3s_2)+\cos 2\pi(3s_1+2s_2)$ $+\cos 2\pi(2s_1+3s_2)+\cos 2\pi(s_1-2s_2)+\cos 2\pi(2s_1-s_2)$
5	$6/\sqrt{3}$	$\cos 6\pi s_1+\cos 6\pi s_2+\cos 6\pi(s_1+s_2)$
	(c) Graphite basal plane: $q=2$, $a_s^*=\sqrt{3}/2$, $\Delta z^*=\dfrac{3.40}{1.42\sqrt{3}}=1.38$	
1	$2/\sqrt{3}$	$-[\cos 2\pi s_1+\cos 2\pi s_2+\cos 2\pi(s_1+s_2)]$
2	2	$2[\cos 2\pi(s_1+2s_2)+\cos 2\pi(2s_1+s_2)+\cos 2\pi(s_1-s_2)]$
3	$4/\sqrt{3}$	$-[\cos 4\pi s_1+\cos 4\pi s_2+\cos 4\pi(s_1+s_2)]$
4	$2\sqrt{7/3}$	$-[\cos 2\pi(3s_1+s_2)+\cos 2\pi(s_1+3s_2)+\cos 2\pi(3s_1+2s_2)$ $+\cos 2\pi(2s_1+3s_2)+\cos 2\pi(s_1-2s_2)+\cos 2\pi(2s_1-s_2)]$
5	$6/\sqrt{3}$	$2[\cos 6\pi s_1+\cos 6\pi s_2+\cos 6\pi(s_1+s_2)]$

Note: for graphite, CC spacing = 1.42 Å in the basal plane, so $a_1=\sqrt{3}\times 1.42=2.46$ Å

In principle, the integrations over s_1 and s_2 can be performed by substituting eq. (2.33) for u_s^* and expanding the exponentials that contain trigonometric functions of s_1 or s_2. We will see in a subsequent section that Henry's Law constants have been calculated for several crystalline surfaces by combining the analytic results for the integrals over s_1 and s_2 that are given in the Appendix with numerical calculations for the limited range of z^* where the analytic expressions are inadequate. The Henry's Law constant will be cal-

culated from

$$K_H = B_{AS}/kT\,. \tag{2.38}$$

It is the reduced gas–solid virial coefficient B^*_{AS} that will be computed in this work; this quantity is defined as $B_{AS}/a_1\mathscr{A}$, where the area of the solid $\mathscr{A}$ is equal to $n_s\, a_s^*\, a_1^2$; B^*_{AS} is thus equal to

$$B^*_{AS} = \int_0^1\int_0^1\int_0^\infty \left[\exp\left(\frac{-u_s^*}{T^*}\right) - 1\right] ds_1\, ds_2\, dz^*. \tag{2.39}$$

We also wish to calculate the average potential energy of an isolated adsorbed atom from eq. (1.5). Additional physical insight is gained if we split the total energy into the average of a τ-independent term, and the average of the Fourier components. We write:

$$\frac{\langle u_s\rangle}{\varepsilon_{gs}} = \langle E_0\rangle + \langle u_\tau\rangle\,, \tag{2.40}$$

where

$$\langle E_0\rangle = \frac{\int_0^1\int_0^1\int_0^\infty E_0(z^*)\exp(-u_s^*/T^*)\, ds_1\, ds_2\, dz^*}{\int_0^1\int_0^1\int_0^\infty [\exp(-u_s^*/T^*) - 1]\, ds_1\, ds_2\, dz^*}, \tag{2.41}$$

$$\langle u_\tau\rangle = \frac{\int_0^1\int_0^1\int_0^\infty \sum_{n>0} E_n(z^*)\, f_n(s_1, s_2)\exp(-u_s^*/T^*)\, ds_1\, ds_2\, dz^*}{\int_0^1\int_0^1\int_0^\infty [\exp(-u_s^*/T^*) - 1]\, ds_1\, ds_2\, dz^*}. \tag{2.42}$$

Details of the analytic evaluations of the integrals over s_1, s_2, in eqs. (2.39), (2.41) and (2.42) are given in the Appendix.

3. Results and discussion

Gas–solid energies were first calculated for the rare gases interacting with the basal plane of graphite. The size and energy parameters for the pairwise potential were estimated using the method of Crowell and Steele[12]), i.e., a geometric mean for ε_{gs} and an arithmetic mean for σ_{gs}, using $\varepsilon_{CC}/k =$

$=28°K$ and $\sigma_{CC}=3.40$ A. Values for $\varepsilon_{gas-gas}/k$ and $\sigma_{gas-gas}$ were taken from Hirschfelder, Curtiss and Bird[13]). The parameters used are shown in table 2, together with the minimum energies over points S, SP and A that were obtained from plots of the summed energies. As can be seen from the curves for He and Ar interacting with this surface that are shown in figs. 2 and 3, the variations in energy with τ are not large. This conclusion is true for the

TABLE 2
Gas–solid energy parameters for rare gas–graphite systems

Gas	ε_{gs}/k (°K)	A	E_0(min)	u_S(min)/ε_{gs}		
				S	SP	A
He	16.9	1.21	−14.08	−14.91	−13.90	−13.76
Ne	31.7	1.25	−15.45	−16.16	−15.28	−15.17
Ar	57.8	1.38	−19.25	−19.73	−19.16	−19.08
Kr	66.6	1.42	−20.16	−20.61	−20.04	−19.99
Xe	79.5	1.52	−22.77	−23.12	−22.69	−22.64

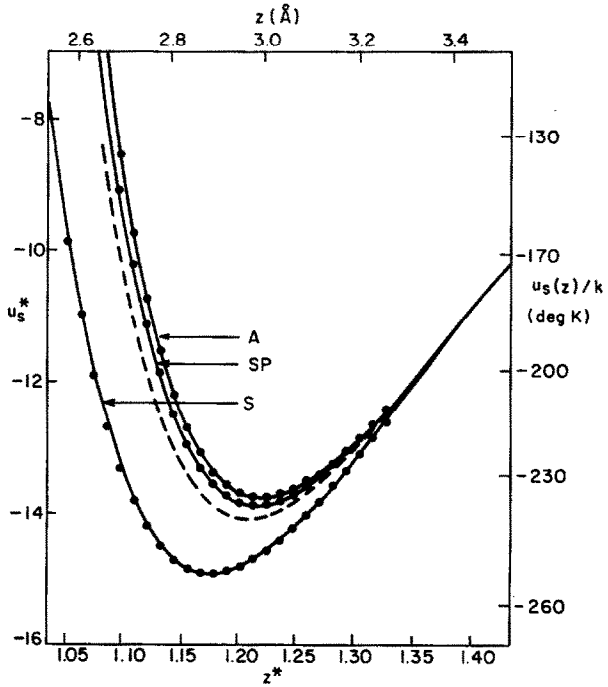

Fig. 2. Gas–solid potential curves for a helium atom at three points over the graphite basal plane. The solid curves were computed by summing the pair-wise He–C energies; the dashed line is E_0, the τ-independent term in the Fourier expansion of u_S, and the points show energies calculated by summing the $n=0$ and the $n=1$ terms

other rare gases which are not shown, and is a well-known feature of previous calculations of gas–graphite energies[14]). The numerical results given in table 2 are comparable with those obtained previously; however, minor differences in the depths of the minima and in variations in energy as the atom translates parallel to the surface are found in the various calculations.

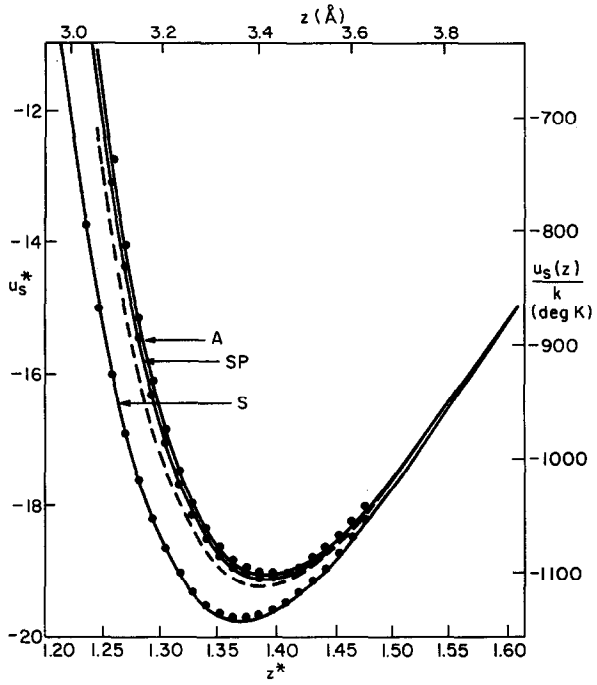

Fig. 3. Gas–solid potential curves for an argon atom interacting with the exposed basal plane of graphite. The curves and points indicate the same quantities as in fig. 2.

These can be ascribed to differences in the choices of potential parameters and functional dependence of the pairwise energy, and to differences in the accuracy of the summation procedure. The fact that the calculations all indicate that the barriers to free translation on this surface are not large has given rise to the current belief that adsorbed layers on this solid are probably the nearest approximation to perfectly mobile films existing in nature. It was found that the inclusion of the $n=1$ term in the Fourier expansion shown in table 1 was adequate to give excellent agreement with the summed energies shown by the solid lines in figs. 2 and 3. The E_0 term in the Fourier expansion is shown by the dashed line, and the points show the

energies given by summing the $n=0$ and the $n=1$ terms for the values of s_1 and s_2 corresponding to points S, A and SP.

Larger lateral variations in energy are exhibited by the pair-wise energy sums for a fcc lattice. Six cases were considered, three gas atom sizes for an exposed (100) face and the same three sizes for a (111) face. The values of A

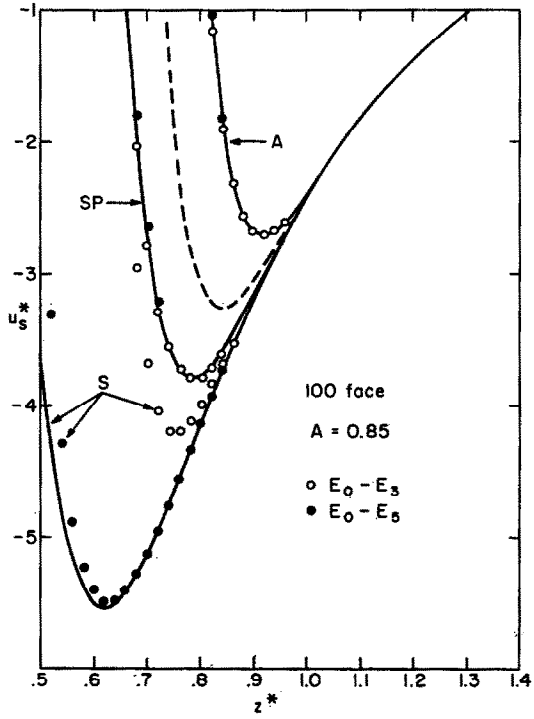

Fig. 4. Potential curves for an atom interacting with the exposed (100) face of an fcc lattice. As in fig. 2, the solid curves are calculated by direct summation, the dashed curve is the $n=0$ term in the Fourier expansion, and the points indicate energies calculated including indicated numbers of terms. At larger distances, the points are not shown, but agree very closely with the summed energies.

chosen were 0.85, 1.00 and 1.20; these correspond to gas atom/solid atom size ratios of approximately 0.7, 1.0 and 1.4, respectively. Figs. 4–9 show the results of a comparison between the truncated Fourier series and the pair-wise sums for three postions of the gas atom over the lattices. It might be noted here that the two sites shown in fig. 1 for the unit cell of the (111) plane are non-equivalent; one site has an atom directly underneath it in the second layer and the other has an atom underneath in the third layer. Al-

though the form of the Fourier series used here does not distinguish between the two positions, this agrees with the direct summations of the pairwise energies for the two sites, since these are essentially identical to each other for all values of the parameters considered in this work. Figs. 4–9 indicate that the number of Fourier terms required to give an accurate representation

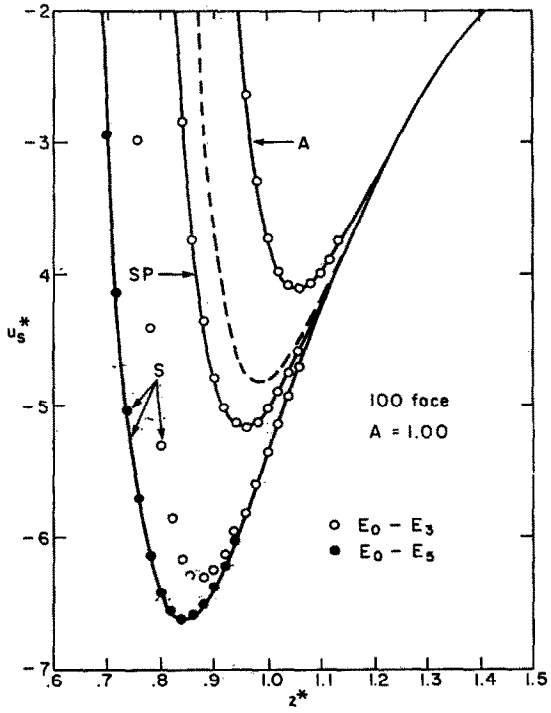

Fig. 5. Energies for a relatively larger gas atom interacting with the same exposed lattice as in fig. 4.

of the energy depends very much upon the size parameter and upon the lattice symmetry, with larger lateral energy variations and more Fourier terms associated with the smallest gas atoms over the looser packed surface lattice. The maximum number of energy terms needed were those with $n \leqslant 5$ for the S position of the smallest gas atom over the (100) face; in all other cases (except possibly the S position with $A = 1.00$, (100) face) $n \leqslant 3$ was adequate (and more than adequate for the case of $A = 1.20$, (111) face). Individual z-dependent coefficients in the Fourier series for the energy are plotted in fig. 10 for $A = 0.85$ over the (111) face. It is evident that the terms with $n \neq 0$

die away quite rapidly with increasing z and with increasing n. The minimum in the τ-independent term E_0 occurs at $z^*=0.85$ and only E_1 is appreciable at this distance; E_0 crosses zero at $z^*=0.72$, and E_1, E_2 and possibly E_3 are appreciable at this distance. Note that E_0 rises quite rapidly with decreasing z, and becomes larger than E_1 at $z^*=0.62$; this means that the total gas–surface energy will become positive for all positions of the gas atom relative

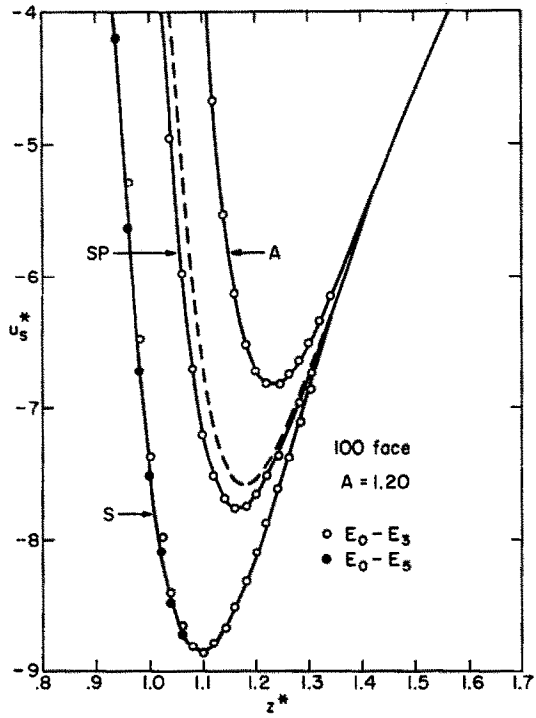

Fig. 6. Energies for an even larger atom than those of figs. 4 and 5 interacting with the same solid.

to the lattice at $z^* \simeq 0.60$. Energies at even smaller values of z^* are of no great physical interest because they correspond to large repulsions and small Boltzmann factors.

Although the use of the Fourier expansion of the gas–solid energy represents a considerable gain in convenience over tabulations of sums, the z-dependence of the coefficients is still in a somewhat awkward form. For the $n=0$ coefficient, the sums over the layers of atoms can generally be terminated with the surface layer for the repulsive part of the energy;

however, the complete sum of the z^{-4} energies with individual planes must be performed if one is to arrive at a proper calculation of the long-range z^{-3} variation of the attractive energy. Furthermore, the modified Bessel functions that appear in the coefficients with $n>0$ are not particularly easy to compute or manipulate. However, it is possible to fit both types of energy to simpler analytic functions with satisfactory accuracy. In particular, it was

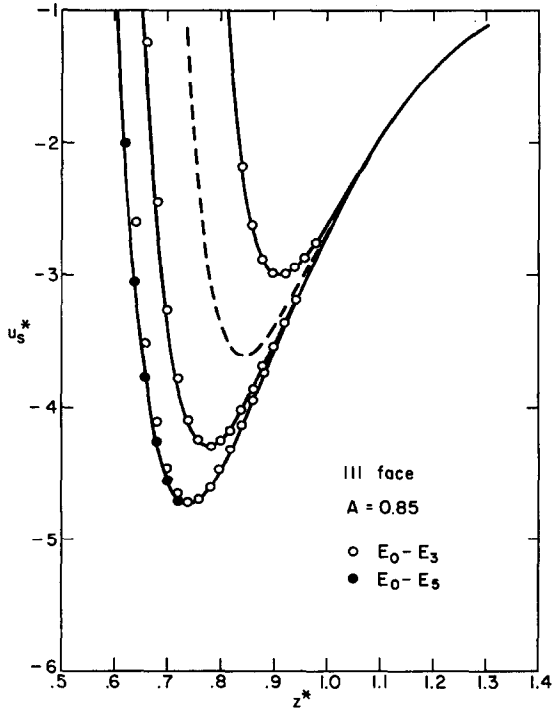

Fig. 7. Energies for a gas atom with a size identical to that of fig. 4, but at three positions over an exposed (111) plane rather than the (100) plane. Curves calculated are the same as in fig. 4, but the positions are those for the unit cell of the (111) lattice shown in fig. 1.

found that the coefficients for the various fcc systems with $n \neq 0$ were exponential functions of z^* over the important range of z^*; parameters of the fit are shown in table 3. The E_0 terms that are shown by the dashed lines in figs. 4–9 are clearly of the general form of an inverse n–m power law or of a Morse potential. Fits to the Morse potential were unsatisfactory; although the variations in energy near the minima were reproduced satisfactorily, it is necessary that these curves also be accurately reproduced

TABLE 3

Constants for analytic representations of the component terms in the gas–solid energy

n		$E_n = \frac{1}{2} b \exp[-a(z^* - z_s^*)], n > 0$					
		$A = 0.85$		$A = 1.00$		$A = 1.20$	
		(111) face	(100) face	(111) face	(100) face	(111) face	(100) face
1	a	19.4	19.4	16.6	16.3	14.3	13.6
	b	42.0	47.0	44.0	53.7	15.8	20.7
	z_s^*	0.6	0.6	0.7	0.7	0.9	0.9
2	a	22.6	20.0	20.8	17.6	19.4	15.6
	b	8.45	24.3	6.05	22.0	0.88	6.05
	z_s^*	0.6	0.6	0.7	0.7	0.9	0.9
3	a	24.8	22.8	22.9	21.2	21.5	19.6
	b	4.45	7.60	2.60	5.43	0.26	0.78
	z_s^*	0.6	0.6	0.7	0.7	0.9	0.9
4	a	29.7	24.3	29.4	22.6	–	21.3
	b	0.72	4.55	0.28	2.80	–	0.31
	z_s^*	0.6	0.6	0.7	0.7	–	0.9
5	a	–	28.1	–	25.1	–	–
	b	–	1.10	–	0.47	–	–
	z_s^*	–	0.6	–	0.7	–	–

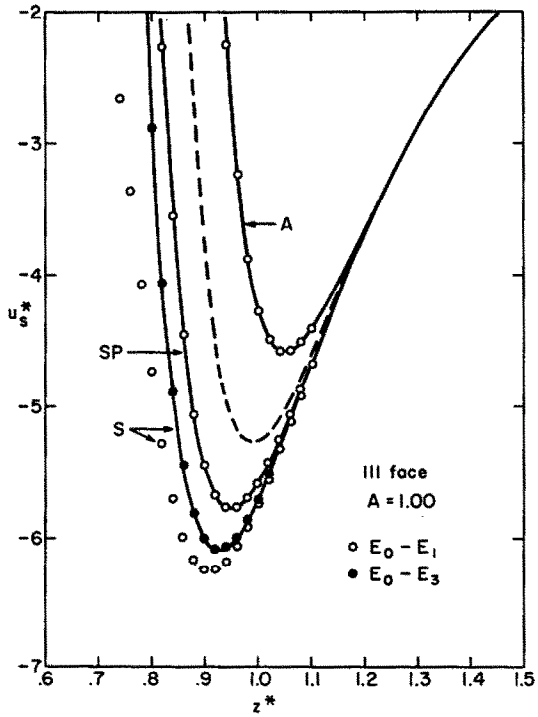

Fig. 8. Energies for an atom of the same size as in fig. 5, but over a (111) plane.

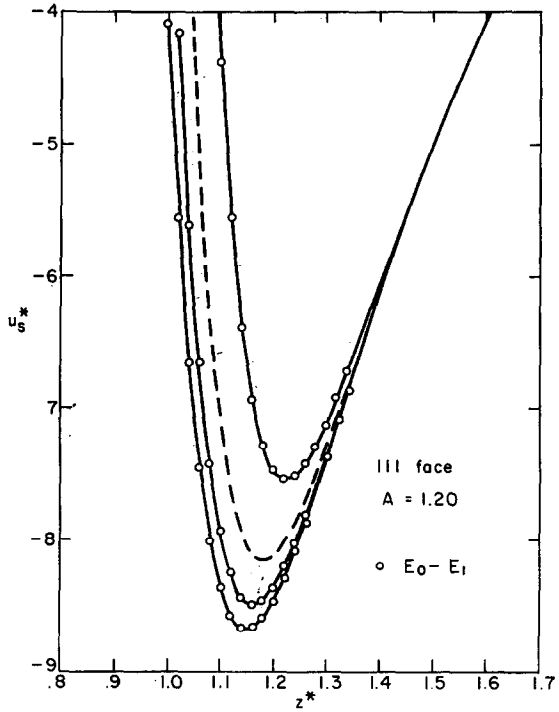

Fig. 9. Potential curves for the atom of fig. 6 but over a (111) plane.

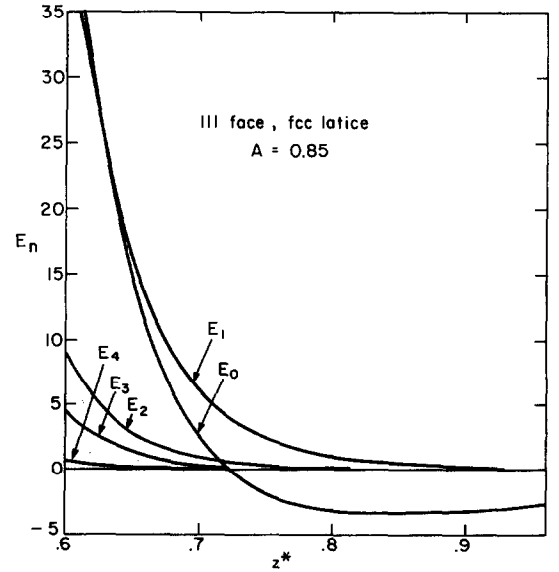

Fig. 10. The separate components of the Fourier expansion of the energy are shown here for the (111) face and the smallest gas atom size considered. Except for E_0, the curves show $2E_n$.

at distances shorter than the minumum; for example, the site on a (100) face with $A=1.00$ has an energy minimum at $z^*=0.84$; at this point, the total energy is made up of a sum of several large terms, with $E_0=0.28, E_1=2.675$, $E_2=0.925$, $E_3=0.14$, $E_4=0.006$, $E_5=0.005$, giving a net energy of -6.62. Evidently, it is important to have an accurate representation of E_0 even when z^* corresponds to positive energies, and the Morse potential fails rather badly by this criterion. However, an excellent approximation to E_0 can be obtained by taking the first terms in the sums over z^{-4} and z^{-10}, neglecting higher terms in the z^{-10} sum, and replacing the remainder of the z^{-4} sum by a term corresponding to the integrated energy. Thus, eq. (2.34) can be replaced by

$$E_0(z^*)=\frac{2\pi qA^6}{a_s^*}\left(\frac{2A^6}{5z^{*10}}-\frac{1}{z^{*4}}-\frac{1}{3\,\Delta z^*(z^*+0.61\,\Delta z^*)^3}\right). \tag{3.1}$$

[It was found that a more accurate representation is obtained if the integration begins at $z^*+0.61\,\Delta z^*$ rather than the value of $z^*+\Delta z^*$ indicated by the sum in eq. (2.34).]

One approximation to the potential curves that is often employed, especially for calculations at low temperatures, is the harmonic oscillator representation of energy changes near the minimum. We can utilize either eq. (2.33) or the approximations to this energy given in eq. (3.1) and table 3 to derive an expression for the force constant k_z for motion in the z-direction. Eqs. (2.33)–(2.35) give

$$\begin{aligned}
k_z &= \left(\frac{\partial^2 u_s}{\partial z^{*2}}\right)_{z^*=z^*_{\min}} \\
&= \frac{8\pi qA^6}{a_s^*}\sum_{p=0}^{\infty}\left(\frac{11\,A^6}{(z^*+p\,\Delta z^*)^{12}}-\frac{5}{(z^*-p\,\Delta z^*)^6}\right)_{z^*=z^*_{\min}} \\
&+\frac{2\pi A^6}{a_s^*}\sum_{n>0}\left[\frac{A^6}{6}\left(\frac{g_n^*}{z^*}\right)^5\left\{\frac{g_n^{*2}}{20}\left[K_7(g_n^*z^*)+2K_5(g_n^*z^*)+K_3(g_n^*z^*)\right]\right.\right. \\
&+\frac{g_n^*}{z^*}\left[K_6(g_n^*z^*)+K_4(g_n^*z^*)\right]+\frac{6}{z^{*2}}K_5(g_n^*z^*)\Bigg\} \\
&-\left(\frac{g_n^*}{z^*}\right)^2\left\{\frac{g_n^{*2}}{2}\left[K_4(g_n^*z^*)+2K_2(g_n^*z^*)+K_0(g_n^*z^*)\right]\right. \\
&\left.\left.+\frac{2g_n^*}{z}\left[K_3(g_n^*z^*)+K_1(g_n^*z^*)\right]+\frac{12}{z^{*2}}K_2(z_n^*z^*)\right\}\right]_{z^*=z_{\min}} f_n(s_1,s_2).
\end{aligned} \tag{3.2}$$

The most logical choice for s_1, s_2 are the coordinates corresponding to point S, the adsorption site; this choice implies that the adsorbed atom is a three-dimensional oscillator. We can define a force constant k_τ^* for motion parallel to the surface by:

$$\frac{u_s(z_{min}, \tau)}{\varepsilon_{gs}} = \begin{cases} \dfrac{u_s(z_{min}, S)}{\varepsilon_{gs}} + \tfrac{1}{2}k_\tau^*[(\Delta s_1)^2 + (\Delta s_2)^2] & \text{((100) face)} \\ \dfrac{u(z_{min}, S)}{\varepsilon_{gs}} + \tfrac{1}{2}k_\tau^*[(\Delta s_1)^2 + (\Delta s_2)^2 + \Delta s_1\, \Delta s_2] & \text{((111) face or graphite basal plane)} \end{cases} \tag{3.3}$$

where Δs_1, Δs_2 denote displacements from point S. The force constant is obtained by differentiating eq. (2.26), and can be written as:

$$k_\tau^* = -4\pi^2 \sum_{n>0} f_n(S)\, V_n\, E_n(z_{min}^*), \tag{3.4}$$

TABLE 4

Weights for terms in the site energy and the parallel force constant

	$f_n(S)/2$		$2V_n$	
n	(100) face	(111 face)	(100) face	(111) face
1	−2	−1.5	1	2
2	+2	+3	2	6
3	+2	−1.5	4	8
4	−4	−3	10	28
5	+2	+3	8	18

TABLE 5

Minimum energies and force constants for gas atoms on an fcc lattice system

		$A=0.85$		$A=1.00$		$A=1.20$	
		(111) face	(100) face	(111) face	(100) face	(111 face)	(100) face
Site S	z_{min}^*	0.740	0.627	0.927	0.843	1.151	1.095
	$\min \frac{u_s}{\varepsilon_{gs}}$	−4.744	−5.500	−6.075	−6.601	−8.638	−8.798
	k_z^*	197	189	202	189	211	198
	k_τ^*	183	2072	92	214	47	71
$n=0$ term in energy	z_{min}^*	0.845	0.842	0.991	0.987	1.183	1.178
	$\min \frac{u_s}{\varepsilon_{gs}}$	−3.612	−3.271	−5.261	−4.815	−8.139	−7.539
	k_z^*	191	172	200	181	213	196

where the coefficients $f_n(s)$ and V_n are listed in table 4. Values of the force constants k_z^* and k_τ^* that were computed for the various fcc systems considered are given in table 5 together with z^*_{min} and the minimum site energies.

An alternative to the three-dimensional harmonic oscillator model for an adsorbed atom is based on the assumption that the atom translates freely parallel to the surface, but vibrates harmonically in the perpendicular direction. However, it is possible to assume either that the minimum energy and force constant k_z^* are those already tabulated for an atom over the site S, or that they arise from the surface-averaged energy. Of course, the use of the Fourier series ensures that the (unweighted) average energy is just the $n=0$ term in the series; the force constants, minimum energies and z^*_{min} are then obtainable from the $n=0$ terms in eqs. (2.33) and (3.2). These calculated values are also shown in table 5.

Having calculated and parameterized the gas–solid potential function for several simple systems, we now wish to utilize the analytic expressions to

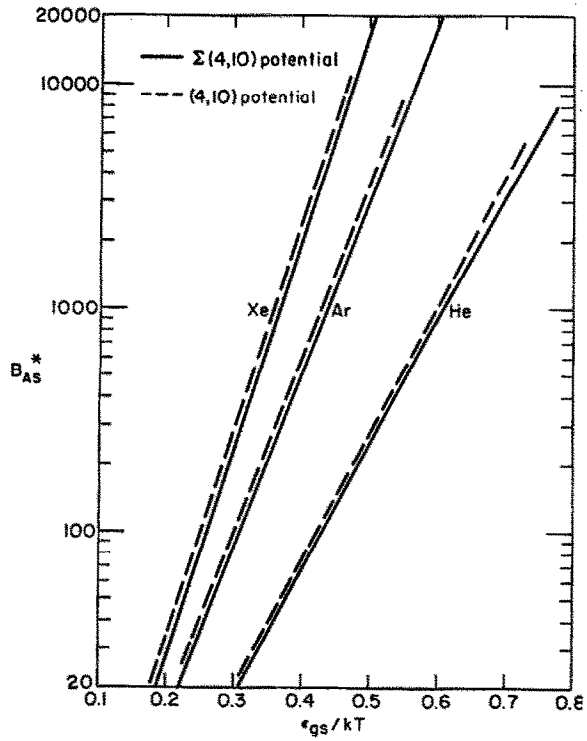

Fig. 11. Reduced gas–solid virial coefficients for rare gases interacting with the graphite basal plane are plotted as a function of the inverse reduced temperature. The solid curves were calculated using the gas–solid potential given by the Fourier expansion including only the τ-dependent terms corresponding to $n=1$.

calculate the single-particle thermodynamic properties discussed in section 2. In the case of the rare gases adsorbed on graphite, the gas–solid virial coefficients were evaluated first using eq. (2.39) for the integral over τ; subsequently the calculation was performed under the assumption that the τ-dependence of the potential was small enough to allow one to use the unweighted average $E_0(z^*)$ in the z-integration. The exact values are plotted in fig. 11; it was found that the approximate values given by

$$B^*_{OS} = \int_0^\infty \{\exp[-E_0(z^*)/kT] - 1\}\, dz^* \tag{3.5}$$

are indistinguishable from B^*_{AS} on the scale of fig. 11.

Gas–solid virial coefficients have been calculated for the (4,10) potential by Yaris and Sams[15]). The quantity actually tabulated by these workers is denoted I_{cl}, and is related to B_{AS} by

$$B_{AS} = s_0 \mathscr{A} I_{cl}, \tag{3.6}$$

where s_0 is the distance where the potential $u_s(z)$ passes through zero. According to eq. (2.28), $s_0 = 0.4^{\frac{1}{6}}\sigma_{gs}$ for the (4, 10) potential. Consequently,

$$B^*_{AS} = 0.4^{\frac{1}{6}}\, A I_{cl}. \tag{3.7}$$

Virial coefficients obtained from eq. (3.7) should be nearly the same as those calculated in this work, since E_0 for the exposed graphite basal plane is a summed (4,10) potential in which contributions from planes more distant than the surface plane are particularly small because of the large inter-planar spacing in this material. Yaris and Sams give I_{cl} as a function of ε_{1s}/kT, where ε_{1s} is equal to E_0 (min) in the present notation. The dashed lines in fig. 11 show B^*_{AS} calculated from their tabulation of I_{cl} using the values of E_0(min) and A given in table 2. We see that the approximate and the exact potentials give very similar results; indeed, it is likely that errors arising from the use of B^*_{AS} for the (4,10) potential in the graphitized carbon black systems will be negligible compared to those associated with other assumptions such as pair-wise additivity and a perfect array of exposed basal planes.

Extensive measurements of B_{AS} have been reported for gases interacting graphite[16]); these data have been compared with the theoretical coefficients calculated for inverse power law potentials in z including (3,9) and (4,10), among others. The present calculations indicate that neglect of the τ-dependence of the energy is justified and that the (4,10) power law is a satisfactory inverse power law representation of the energy for these systems.

The potential curves for the fcc lattice show that the τ-dependence of these energies is considerably more important than for the graphite basal plane.

In fact, the variations become quite large for z^* less than $z^*_{min}+0.15$, where z^*_{min} is the distance of the minimum in E_0.

In calculating thermodynamic quantities for these systems, numerical integrations over s_1 and s_2 were performed for z^* ranging from $z^*_{min}+0.15$ to $z^*_{min}-0.15$; the analytic expressions derived in the Appendix were used for larger z^*; the Boltzmann factors in eqs. (2.39), (2.41) and (2.42) were taken to be zero for smaller z^*. As an illustration of the behavior of the integrands in these equations, $\Omega(z^*, T^*)$ is plotted in fig. 12 for one temperature and

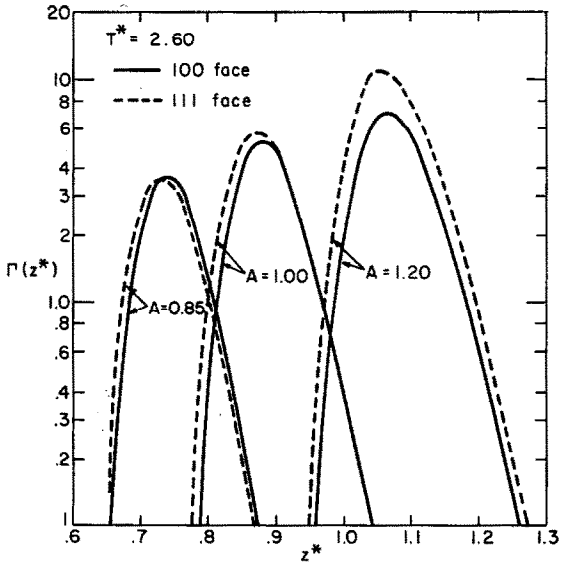

Fig. 12. The parameter Γ is defined by eq. (2.35), and is equal to: the integral at fixed z^* of the τ-dependent part of the gas–solid energy times the Boltzmann factor for the entire energy. It is plotted here on a logarithmic scale for an intermediate value of T^*; for lower temperatures, the variations in Γ are even steeper and more localized. By reference to figs. 4–9, it can be seen that the maxima occur at values of z^* that are generally intermediate between the distances for the minimum energies at points S and SP.

several surfaces. According to the definition given for this quantity in eq. (A.14), it is proportional to the surface-average of the τ-dependent terms in the energy. The average is weighted by exp $(-u^*_s/T^*)$, and thus contains E_0/T^* as well as the τ-dependent energy. Fig. 12 shows that this function varies quite rapidly with z^*, and becomes quite small for z^* outside the limited range where numerical integration is employed in calculating the average over s_1 and s_2.

Computed values of B^*_{AS} are listed in table 6 for the fcc systems considered.

TABLE 6

B_{AS}^* values for fcc surface lattices

kT/ε_{gs}	(100) face			(111 face)		
	$A=0.85$	$A=1.00$	$A=1.20$	$A=0.85$	$A=1.00$	$A=1.20$
0.6667	66.45			69.09		
0.7	50.26			52.98		
0.75	34.81	214.45		37.26	267.84	
0.8	25.36	140.69		27.44	175.09	
0.9	15.05	70.49		16.51	86.90	
1.0	9.939	40.95	498.21	10.991	49.94	742.71
1.2	5.282	18.30	149.63	5.887	21.89	209.42
1.5	2.679	8.111	46.10	3.008	9.500	60.48
2.0	1.176	3.359	14.25	1.342	3.869	17.60
2.6	0.508	1.598	6.038	0.605	1.837	7.211
3.2	0.192	0.856	3.296	0.258	0.997	3.883
4.0	−0.033	0.365	1.743	0.012	0.449	2.053
5.0	−0.186	0.051	0.865	−0.156	0.102	1.041
6.4	−0.303	−0.178	0.284	−0.283	−0.149	0.385
8.0	−0.378	−0.319	−0.049	−0.364	−0.302	0.015

These results are plotted in fig. 13, where they are compared with two approximate calculations. The first of these consists in replacing the τ-average of $\exp[-u_s(r)/kT]$ by the exponential of the τ-average of $-u_s(r)/kT$. Of course, the τ-average of $u_s(r)/\varepsilon_{gs}$ is just $E_0(z^*)$, so that the dashed lines in the figures represent B_{OS}^*. The differences between B_{AS}^* and B_{OS}^* become larger as the relative size of the gas atom decreases, as one might expect; in addition, the differences for a fixed size ratio are slightly larger for the exposed (100) plane than for the close-packed (111) plane. The low temperature harmonic oscillator approximation was also used to compute B_{AS}^*; this gives

$$B_{AS}^* = \frac{(2\pi kT)^{\frac{3}{2}}}{(k_z^*)^{\frac{1}{2}}\, k_\tau^*} \exp\left(\frac{-E_{min}(S)}{T^*}\right) \tag{3.6}$$

for a three-dimensional oscillator, where $E_{min}(S)$ is the minimum energy at a site. Alternatively,

$$B_{OS}^* = \left(\frac{2\pi kT}{k_z^*}\right)^{\frac{1}{2}} \exp\left(\frac{-E_{min}(0)}{T^*}\right) \tag{3.7}$$

for a one-dimensional oscillator. In eq. (3.7), we have once again replaced the average of the exponential by the exponential of the average; consequently, k_z^* in eq. (3.7) is equal to the curvature of $E_0(z^*)$, and $E_{min}(0)$ is the minimum value of this function. In contrast, the force constants in eq. (3.6) refer to the curvature of $u_s(r)$ at a site; as is shown in table 5, the force constant

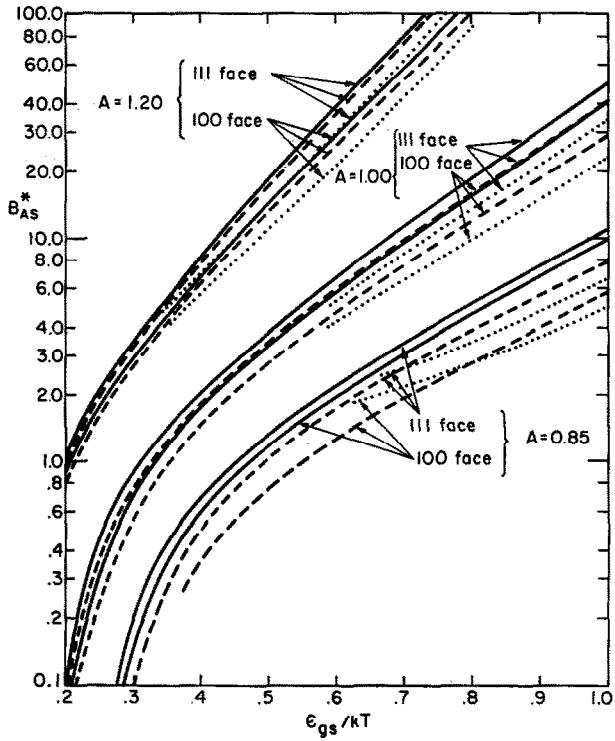

Fig. 13. Reduced virial coefficients are plotted here as a function of the inverse reduced temperature for the various gas–fcc solid systems considered. The solid lines denote calculations carried out using the Fourier expansion for the energy including all terms up to and including $n = 5$; the dashed lines denote the results obtained when only the $n = 0$ term was taken; and the dotted lines are the low-temperature harmonic-oscillator approximations to the $n = 0$ calculation.

k_z^* required in eq. (3.6) is not quite the same as that for eq. (3.7). It was found that the three-dimensional harmonic oscillator model of eq. (3.6) was an extremely poor representation of B^*_{AS} for these systems, but that eq. (3.7) gives moderately good results at low temperatures, as shown by the dotted lines in fig. 13. Of course, these curves really give an approximation to the dashed lines which show B^*_{OS} calculated from eq. (3.5).

It is not difficult to include a computation of the average potential energy $\langle u_s(r)\rangle$ in the computer program for B^*_{AS}. Energies obtained in this way can be compared with the harmonic oscillator approximation. One should find that

$$\langle \delta E\rangle = \frac{\langle u_s(r)\rangle}{\varepsilon_{gs}} - E_{min}(S) = \tfrac{3}{2}T^* \tag{3.8}$$

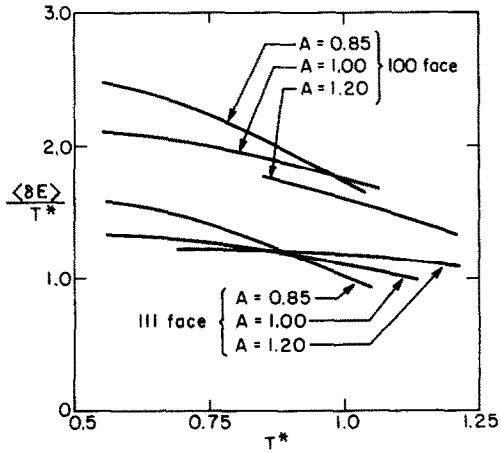

Fig. 14. The ratio of the average energies of adsorbed gas atoms to the reduced temperature are shown here for low temperatures. The energy $\langle \delta E \rangle$ is the energy in excess of $E_{\min}(S)$.

for a three-dimensional oscillator, or

$$\langle \delta E \rangle = \frac{\langle u_s(\boldsymbol{r}) \rangle}{\varepsilon_{gs}} - E_{\min}(0) = \tfrac{1}{2} T^* \tag{3.9}$$

for the one-dimensional oscillator model. Fig. 14 shows plots of the computed $\langle \delta E \rangle / T^*$ at low temperatures. It is evident that these energies do not correspond very well to the one-dimensional oscillator model; the three-dimensional model is considerably worse. Evidently, the τ-dependence of $u_s(\boldsymbol{r})$ makes an important contribution to $\langle \delta E \rangle$; consequently, it is larger than $\frac{1}{2} T^*$; however, this part of $u_s(\boldsymbol{r})$ is sufficiently anharmonic to invalidate the three-dimensional oscillator representation at the temperatures considered here. It is interesting to note that the energies for the (100) face fall into a group that is noticeably larger than those for the (111) face; this is consistent with the conclusion that the τ-dependent terms make an important contribution to $\langle \delta E \rangle$, since these terms are generally larger for the (100) face than the (111) face.

4. Conclusions

After developing the formalism necessary to obtain an analytic expression for pair-wise additive gas–solid energies, extensive calculations of potentials and thermodynamic properties have been presented. The primary reasons for performing such computations are two-fold: (1) to illustrate the utility of the analytic expressions, and (2) to explore the validity of some common approximations for the thermodynamic properties of isolated adsorbed

atoms. It is now possible to conclude that the Fourier expansion approach to the calculation of gas–solid potentials is indeed of considerable practical utility, and that the number of terms required to give accurate energies is not inconveniently large. Future publications will be concerned with the use of these expressions to calculate second and third virial coefficients of atoms adsorbed on crystal surfaces, and with molecular beam scattering, and will provide additional demonstrations of the power and convenience of this approach.

Of the various systems studied here, it was found that the properties of the rare gases interacting with graphite do not differ noticeably from those suggested previously; however, the calculation of B_{AS}^{*} for graphite surfaces has been performed here for the first time with a potential that includes the τ-dependent terms in the energy. In the case of the fcc lattice, previous work has been quite limited, on both the potentials and the gas–solid virial coefficients. For the range of gas/solid atomic size ratios considered here, it can now be seen that the barrier to free translation on either crystal face is appreciable, but not high enough to cause an adsorbed atom to behave as a three-dimensional harmonic oscillator (at temperatures considered in this calculation); in addition, the differences between the adsorptive properties of the (100) face and the (111) face have been explicitly calculated; it is evident that the techniques developed here can be applied to treat other exposed lattice planes if so desired. Inasmuch as the surfaces of most crystalline solid adsorbents consist of a mixture of various exposed lattice planes, these calculations are basic to treatments of the adsorption heterogeneity associated with such mixtures. For example, the Henry's Law constant (or B_{AS}) for these adsorbents is equal to an appropriately weighted average of the constants for the various exposed planes. With the increasing use of LEED for determining surface lattice size and symmetry[17]), it appears that calculations of such averages may become feasible for real adsorbents in the near future.

Appendix

Explicit expressions will be derived here for some of the thermodynamic parameters that that characterize the isolated atom adsorbed on the surface of a perfect crystal. The quantities to be calculated are the Henry's Law constant [given by eq. (2.37)] and/or the average potential energy of the adsorbed atom given by eqs. (2.40)–(2.42). It will be assummed that the Fourier series for the gas–solid energy has been expressed as:

$$u_s^*(\boldsymbol{r}) = \sum_{\boldsymbol{g}} E_{\boldsymbol{g}} \cos(\boldsymbol{g}\cdot\boldsymbol{\tau}), \tag{A.1}$$

where the coefficients $E_{\boldsymbol{g}}$ are functions of z, and will generally be expressed

in terms of the symmetry variables s_1 and s_2. Eq. (A.1) is thus a slightly modified version of eq. (2.33) in which the trigonometric functions in $f_n(s_1, s_2)$ are shown explicity. The exponential that appears in the integrand of eq. (2.37) can now be written as:

$$\exp\left(\frac{-u_s^*}{T^*}\right) = \exp\left(\frac{-E_0}{T^*}\right) \prod_{\boldsymbol{g}\neq 0} \exp\left(\frac{-E_{\boldsymbol{g}}\cos(\boldsymbol{g}\cdot\boldsymbol{\tau})}{T^*}\right). \tag{A.2}$$

The exponentials with non-zero $\boldsymbol{g}$ can be expanded as infinite series:

$$\exp\left(\frac{-E_{\boldsymbol{g}}\cos(\boldsymbol{g}\cdot\boldsymbol{\tau})}{T^*}\right) = I_0\left(\frac{-E_{\boldsymbol{g}}}{T^*}\right) + 2\sum_{m=1}^{\infty} I_m\left(\frac{-E_{\boldsymbol{g}}}{T^*}\right)\cos(m\boldsymbol{g}\cdot\boldsymbol{\tau}), \tag{A.3}$$

where I_m is a modified Bessel function of the first kind, and thus has the property that $I_m(-x)=(-1)^m I_m(x)$.

When eq. (A.3) is substituted into eq. (A.2), the result is

$$\begin{aligned}\exp\left(\frac{-u_s^*}{T^*}\right) = \exp\left(\frac{-E_0}{T^*}\right)\Bigg\{&\prod_{\boldsymbol{g}\neq 0} I_0\left(\frac{-E_{\boldsymbol{g}}}{T^*}\right) \\ &+ 2\sum_{\boldsymbol{g}'\neq 0}\sum_{m'=1}^{\infty} I_{m'}\left(\frac{-E_{\boldsymbol{g}'}}{T^*}\right)\cos(m'\boldsymbol{g}'\cdot\boldsymbol{\tau})\prod_{\boldsymbol{g}\neq 0,\,\boldsymbol{g}'} I_0\left(\frac{-E_{\boldsymbol{g}}}{T^*}\right) \\ &+ 4\sum_{\boldsymbol{g}'\neq 0,\,\boldsymbol{g}''}\sum_{\boldsymbol{g}''\neq 0}\sum_{m'=1}^{\infty}\sum_{m''=1}^{\infty} I_{m'}\left(\frac{-E_{\boldsymbol{g}'}}{T^*}\right) I_{m''}\left(\frac{-E_{\boldsymbol{g}''}}{T^*}\right) \\ &\times\cos(m'\boldsymbol{g}'\cdot\boldsymbol{\tau})\cos(m''\boldsymbol{g}''\cdot\boldsymbol{\tau})\prod_{\boldsymbol{g}\neq 0,\,\boldsymbol{g}',\,\boldsymbol{g}''} I_0\left(\frac{-E_{\boldsymbol{g}}}{T^*}\right) + \cdots\Bigg\}.\end{aligned} \tag{A.4}$$

For example, consider the gas–graphitized carbon black systems where an adequate representation of the energy is obtained if one includes only three terms; namely with those $g_1, g_2 = 0, 1;\ 1, 0;$ and $1, 1$. Since the coefficient in the energy equation has been denoted by $-E_1$ for these terms, one has:

$$\begin{aligned}\exp\left[\left(\frac{-u_s^*}{T^*}\right)\right]_{\text{graphite}} = 2\exp\left(\frac{-E_0}{T^*}\right)\Bigg\{&\frac{1}{2}\left[I_0\left(\frac{E_1}{T^*}\right)\right]^3 \\ &+ 2\left[I_0\left(\frac{E_1}{T^*}\right)\right]^2\sum_{m'=1}^{\infty} I_{m'}\left(\frac{E_1}{T^*}\right) \\ &\times\left[\cos(2\pi m' s_1) + \cos(2\pi m' s_2) + \cos(2\pi m'(s_1+s_2))\right] \\ &+ 4I_0\left(\frac{E_1}{T^*}\right)\sum_{m'=1}^{\infty}\sum_{m''=1}^{\infty} I_{m'}\left(\frac{E_1}{T^*}\right) I_{m''}\left(\frac{E_1}{T^*}\right) \\ &\times\left[(\cos(2\pi m' s_1)\cos(2\pi m'' s_2)\right) \\ &+ \left(\cos(2\pi m' s_1) + \cos(2\pi m' s_2)\right)\cos(2\pi m''(s_1+s_2))\right] \\ &+ 8\sum_{m'=1}^{\infty}\sum_{m''=1}^{\infty}\sum_{m'''=1}^{\infty} I_{m'}\left(\frac{E_1}{T^*}\right) I_{m''}\left(\frac{E_1}{T^*}\right) I_{m'''}\left(\frac{E_1}{T^*}\right) \\ &\times\cos(2\pi m' s_1)\cos(2\pi m'' s_2)\cos(2\pi m'''(s_1+s_2))\Bigg\}.\end{aligned} \tag{A.5}$$

The advantage of these series is of course that they contain orthogonal functions of s_1, s_2. Consequently, considerable simplification occurs when integrations over these variables are performed. We define

$$\Gamma(z^*, T^*) = \int_0^1 \int_0^1 \exp\left(\frac{-u_s^*}{T^*}\right) ds_1\, ds_2 . \tag{A.6}$$

In the graphitized carbon black systems, it emerges that:

$$\Gamma(z^*, T^*)]_{\text{graphite}} = \exp\left(\frac{-E_0}{T^*}\right)\left\{\left[I_0\left(\frac{E_1}{T^*}\right)\right]^3 + 4\sum_{m=1}^{\infty}\left[I_m\left(\frac{E_1}{T^*}\right)\right]^3\right\}. \tag{A.7}$$

In the general case, the integrations over s_1, s_2 yield an expression of the form:

$$\Gamma(z^*, T^*) = \exp\left(\frac{-E_0}{T^*}\right)\left\{\prod_{g\neq 0} I_0\left(\frac{-E_g}{T^*}\right) + 2\prod_{g\neq 0,\, g',\, g''} I_0\left(\frac{-E_g}{T^*}\right)\sum_{m'=1}^{\infty}\sum_{m''=1}^{\infty} I_{m'}\left(\frac{-E_{g'}}{T^*}\right) I_{m''}\left(\frac{-E_{g''}}{T^*}\right)\delta_{m'g',\, m''g''} + \cdots\right\}, \tag{A.8}$$

where the Kronecker δ denotes

$$\delta_{m'g',\, m''g''} = \delta_{m'g_1',\, m''g_1''}\, \delta_{m'g_2',\, m''g_2''} . \tag{A.9}$$

Evidently, the utility of this approach is quite dependent upon the number of Fourier terms required to adequately represent u_s, as well as the number of Bessel functions required to adequately represent each factor in $\exp(-u_s^*/T^*)$ In fact, both of these numbers change quite rapidly as z^*, the third integration variable, changes. As z^* increases, one generally passes through a region where it is more convenient to integrate numerically over s_1 and s_2 than to make use of the series expansions of the integrand. However, this region is small; for example, in the fcc systems considered here, the range of poor convergence is typically from $z^* = z^*_{\min} - 0.15$ to $z^*_{\min} + 0.15$ where $z^*_{\min}$ is the distance of the minimum energy for position S. At smaller z^*, E_0 increases so rapidly that it overwhelms the sum of Fourier terms with $\boldsymbol{g \neq 0}$, and $\exp(-u_s^*/T^*)$vanishes at all s_1, s_2. At larger z^* for the fcc systems, it is convenient to write the integrals over s_1, s_2 in terms of the analytic expressions for these lattices. Specifically, if z^* is large enough so that the Fourier terms with $n > 1$ can be neglected for the (111) face, fcc lattice, it is easy to show that the expression that results for $\Gamma(z^*, T^*)$ is identical to eq. (A.7) except for a sign change in the arguments of the Bessel functions. On the other hand, the τ-dependent terms are generally larger for the (100) face, fcc lattice than for the (111) face. If it is assumed that the terms for $g_1, g_2 = 0, +1$

and $\pm 1,0(E_1)$ and for $g_1, g_2 = 1, \pm 1$ and $-1, \pm 1(E_2)$ are important, but that all other Fourier components make a negligible contribution, eq. (A.8) becomes

$$\Gamma(z^*, T^*)]_{100\,\text{face, fcc}} = 2\exp\left(\frac{-E_0}{T^*}\right)\left\{\frac{1}{2}\left[I_0\left(\frac{-E_1}{T^*}\right)I_0\left(\frac{-E_2}{T^*}\right)\right]^2\right.$$
$$+ 4I_0\left(\frac{-E_2}{T^*}\right)\sum_{m=1}^{\infty} I_m\left(\frac{-E_2}{T^*}\right)\left[I_m\left(\frac{-E_1}{T^*}\right)\right]^2$$
$$+ 4I_0\left(\frac{-E_1}{T^*}\right)\sum_{m=1}^{\infty} I_{2m}\left(\frac{-E_1}{T^*}\right)\left[I_m\left(\frac{-E_2}{T^*}\right)\right]^2$$
$$\left. + 8\sum_{m=1}^{\infty}\sum_{m'=1}^{\infty} I_{m+m'}\left(\frac{-E_1}{T^*}\right)I_{m-m'}\left(\frac{-E_1}{T^*}\right)I_m\left(\frac{-E_2}{T^*}\right)I_{m'}\left(\frac{-E_2}{T^*}\right)\right\}. \quad \text{(A.10)}$$

[Higher order terms that would appear in the general expression are absent in eq. (A.10) because of our assumption that only four Fourier terms need be taken to represent $u_s(\boldsymbol{r})$ in pertinent range of z^*.]

These expressions for $\Gamma(z^*, T^*)$ can be used to calculate the gas–solid virial coefficient B^*_{AS} defined in eqs. (2.38) and (2.39). One has

$$B^*_{AS} = \int_0^{\infty} [\Gamma(z^*, T^*) - 1]\,\mathrm{d}z^*. \quad \text{(A.11)}$$

The energies defined in eq. (2.40) are given by

$$\langle E_o \rangle = \frac{\int_0^{\infty} E_0(z^*)\,\Gamma(z^*, T^*)\,\mathrm{d}z^*}{\int_0^{\infty} [\Gamma(z^*, T^*) - 1]\,\mathrm{d}z^*}, \quad \text{(A.12)}$$

and

$$\langle u_\tau \rangle = \frac{\int_0^{\infty} \Omega(z^*, T^*)\,\mathrm{d}z}{\int_0^{\infty} [\Gamma(z^*, T^*) - 1]\,\mathrm{d}z^*}, \quad \text{(A.13)}$$

where

$$\Omega(z^*, T^*) = \sum_{\boldsymbol{g}\neq\boldsymbol{0}} E_{\boldsymbol{g}}(z^*)\int_0^1\int_0^1 \cos(\boldsymbol{g}\cdot\boldsymbol{\tau})\exp\left(\frac{-u_s^*}{T^*}\right)\mathrm{d}s_1\,\mathrm{d}s_2. \quad \text{(A.14)}$$

One can use eq. (A.4) together with the orthogonality properties of the cosine factors to evaluate the integrals over s_1 and s_2 in eq. (A.14); the resulting expression for $\Omega(z^*, T^*)$ can be written as:

$$\Omega(z^*, T^*) = \exp\left(\frac{-E_0}{T^*}\right)\left\{\sum_{g' \neq 0}\sum_{g'' \neq 0} E_{g'}\left[I_1\left(\frac{-E_{g''}}{T^*}\right)\delta_{g', g''} + I_2\left(\frac{-E_{g''}}{T^*}\right)\delta_{g', 2g''} + \cdots\right]\prod_{g=0, g''} I_0\left(\frac{-E_g}{T^*}\right) + \cdots\right\}. \quad \text{(A.15)}$$

Specific results include:

$$\Omega(z^*, T^*)]_{\text{graphite}} = 2\exp\left(\frac{-E_0}{T^*}\right)E_1\left\{3\left[I_0\left(\frac{E_1}{T^*}\right)\right]^2 I_1\left(\frac{E_1}{T^*}\right) + 2\sum_{m=1}^{\infty}\left[I_m\left(\frac{E_1}{T^*}\right)\right]^2\left[I_{m+1}\left(\frac{E_1}{T^*}\right) + I_{m-1}\left(\frac{E_1}{T^*}\right)\right]\right\}. \quad \text{(A.16)}$$

If E_2 and higher Fourier components are negligible, the corresponding expression for the (111) face, fcc lattice is identical to eq. (A.16) except for a sign change in E_1.

Some of the leading terms in the expression for the (100) face include:

$$\begin{aligned}\Omega(z^*, T^*)]_{100\text{ face, fcc}} = 2\exp\left(\frac{-E_0}{T^*}\right)\Bigg\{&2E_1 I_1\left(\frac{-E_1}{T^*}\right)\\ &\times\left[I_0\left(\frac{-E_1}{T^*}\right)\left[I_0\left(\frac{-E_2}{T^*}\right)\right]^2 + 2\sum_{m=1}^{\infty} I_m\left(\frac{-E_1}{T^*}\right)\right.\\ &\left.\times\left[I_m\left(\frac{-E_2}{T^*}\right)\right]^2\right] + 2E_2 I_1\left(\frac{-E_2}{T^*}\right)\left[I_0\left(\frac{-E_2}{T^*}\right)\right.\\ &\left.\times\left[I_0\left(\frac{-E_1}{T^*}\right)\right]^2 + 2\sum_{m=1}^{\infty} I_m\left(\frac{-E_2}{T^*}\right)\left[I_m\left(\frac{-E_1}{T^*}\right)\right]^2\right]\\ &+ 4E_1 I_1\left(\frac{-E_1}{T^*}\right)\sum_{m=1}^{\infty} I_{2m}\left(\frac{-E_1}{T^*}\right)\\ &\times\left[I_m\left(\frac{-E_2}{T^*}\right)\right]^2 + \cdots\Bigg\}. \quad \text{(A.17)}\end{aligned}$$

References

1) W. A. Steele, Advan. Colloid Interface Sci. **1** (1967) 3.
2) R. A. Pierotti, in: *Surface and Colloid Science*, Vol. 4, Ed E. Matijevic (Wiley–Interscience, New York, 1971) p. 93.
3) W. A. Steele and M. Ross, J. Chem, phys. **60** (1961) 850.
4) W. A. Steele, in: *The Solid–Gas Interface*, Vol. 1, Ed. E. A. Flood (M. Dekker, New York, 1966).
5) W. A. Steele and E. Kebbekus, J. Chem. Phys. **43** (1965) 292.
6) F. Ricca, C. Pisani and E. Garrone, in *Proc. Second Intern. Symp. on Adsorption – Desorption Phenomena* (Academic Press, New York, 1972); J. Chem. Phys. **51** (1969) 4079;
   A. D. Novaco and F. J. Milford, J. Low Temp. Phys. **3** (1970) 307.
7) A. D. Novaco and F. J. Milford, Phys. Rev. A **5** (1972) 783.
8) E. C. Beder, in: *Advances in Atomic and Molecular Physics*, Vol. 3 (Academic Press, New York, 1967) p. 205;
   N. Cabrera, V. Celli, F. O. Goodman and R. Manson, Surface Sci. **19** (1970) 67;
   F. O. Goodman, Surface Sci. **19** (1970) 93.
9) J. Hove and J. A. Krumhansl, Phys. Rev. **92** (1953) 569.
10) However, see F. O. Goodman, J. Chem. Phys. **56** (1972) 4899;
    A. Tsuchida, Surface Sci. **14** (1969) 375.
11) J. E. Lennard-Jones and B. M. Dent, Trans Faraday Soc. **24** (1928) 92.
12) A. D. Crowell and R. B. Steele, J. Chem. Phys. **34** (1961) 1347.
13) J. O. Hirschfelder, C. F. Curtiss and R. B. Bird, *Molecular Theory of Gases and Liquids* (Wiley, New York, 1954).
14) A. D. Crowell and D. M. Young, Trans. Faraday Soc. **49** (1953) 1080;
    E. L. Pace, J. Chem. Phys. **27** (1957) 1341;
    N. N. Avgul, A. A. Isirikyan, A. V. Kiselev, I. A. Lygina and D. P. Poshkus, Izv. Akad. Nauk SSSR, Otd. Khim. Nauk. (1957) 1314;
    N. N. Avgul, A. V. Kiselev, I. A. Lygina and D. P. Poshkus, Bull. Acad. Sci. USSR, Div. Chem. Sci. (English Trans.) (1959) 1155;
    R. H. van Dongen, Ph. D. thesis, Technische Hogeschool Delft, 1972;
    W. A. Steele and R. Karl, J. Colloid Interface Sci. **28** (1960) 397.
15) R. Yaris and J. R. Sams, Jr., J. Chem. Phys. **37** (1962) 571.
16) J. R. Sams, Jr., G. D. Halsey, Jr. and G. Constabaris, J. Phys. Chem. **64** (1960) 1689;
    G. Constabaris, J. R. Sams, Jr. and G. D. Halsey, Jr., J. Phys. Chem. **65** (1961) 367;
    J. R. Sams, Jr., G. Constabaris and G. D. Halsey, Jr., J. Chem. Phys. **36** (1962) 1334;
    N. N. Avgul and A. V. Kiselev, in: *Chemistry and Physics of Carbon*, Vol. 6, Ed. P. Walker, Jr. (M. Dekker, New York, 1971).
17) J. W. May, Advan. Catalysis **21** (1970) 151.